Trajectory optimization of unmanned aerial vehicle in dynamic soaring

Bing-Jie Zhu[1, 2], Zhong-Xi Hou[1], Hua-Jiang Ouyang[2]

(1 National University of Defense Technology, Changsha, Hunan, 410073, People's Republic of China; 2 University of Liverpool, Liverpool, L69 3GH, UK)

Abstract: An aircraft can extract energy from a gradient wind field by dynamic soaring. The paper presents trajectory optimization of a UAV (unmanned aerial vehicle) for dynamic soaring by numerical analysis and validates the theoretical work through flight test. The collocation approach is used to convert the trajectory optimization problem into parameters optimization. The control and state parameters include lift coefficient, bank angle, positions, flight path angle, heading angle and airspeed, which are obtained from the parameter optimization software. To validate the results of numerical simulation, the dynamic soaring experiment is also performed and experimental data is analysed. This research work shows that the UAV can gain enough flight energy from the gradient wind field by following an optimal dynamic soaring trajectory. Meanwhile, the variation of flight path angle, heading angle and airspeed has a significant influence on the energy transform. The solution can provide theoretical guide to UAVs for extracting maximum energy from gradient wind fields.

Key words: trajectory optimization; gradient wind field; parameters optimization; dynamic soaring experiment

1 Introduction

The energy requirements of near space UAVs' propulsion and payload systems impose a severe restriction of their effectiveness. Many near space UAVs for observation missions are primarily limited to short range flights due to limited energy supply. In order to extend the flight

[1,2] Bing-Jie Zhu, PhD candidate, College of Aerospace Sciences and Engineering, National University of Defense Technology, Changsha, 410073, China (Email: jackerzhu@163.com)

[1]Zhong-Xi Hou, professor, College of Aerospace Sciences and Engineering, National University of Defense Technology, Changsha, 410073, China Email: hzx@nudt.edu.cn

[2]Hua-Jiang Ouyang, professor, School of Engineering, University of Liverpool, UK. Email: h.ouyang@liverpool.ac.uk

time and flight distance, certain energy existing in the flight environment such as solar energy can be considered, which lead to the design of large aspect-ratio high-altitude long-endurance UAVs. But during evening time, when there is no solar light, because of the limitation of energy storage battery, the solar energy absorbed in daytime cannot keep up with the energy consumption for night flying [1]. On the other hand, some other forms of environmental energy can be resorted to, such as gradient wind energy [2]. According to observation data, taken at the altitude of 25 km, there is a steady gradient wind field, with wind speed gap of about 5 m/s [3]. Exacting energy from a gradient wind is generally referred to as dynamic soaring. If a high-altitude long-endurance aircraft can cruise in near space without propulsive thrust or little power by means of dynamic soaring at night, the aircraft would stay in the air for more than one month. As a matter of fact, there are many large-sized birds make use of gradient wind to enhance their flight ability in nature, e.g. albatross [4]. An illustration of a typical dynamic soaring style of albatross is shown in Figure 1. The dynamic soaring cycle can be divided into four phases: climbing with headwind, turning in high altitude, gliding with tailwind, turning at low altitude [5], as shown in Figure 1 (b).

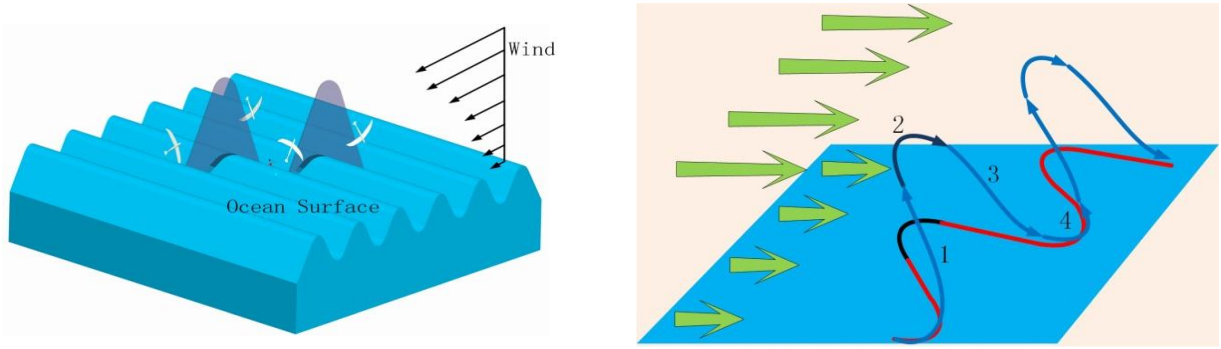

(a) (b)

Figure 1. Trajectory used by the albatross for dynamic soaring

The Wandering Albatross lives predominantly in Kerguelen Archipelago of the southern hemisphere, which makes use of dynamic soaring to travel throughout the South Ocean with little propulsive energy expenditure. Early in 1883, Lord Rayleigh [6] published “The soaring of birds” on

the Nature, which is regarded as the first paper about dynamic soaring. Nowadays, there are a lot of missions that the soaring UAVs would be well suited to perform. The first would be a science platform to collect data on the interactions between the ocean and lower atmosphere, which is of interest to climate scientists as significant momentum and energy are transferred across this interface [7]. A dynamic soaring UAV would also provide a reasonable observation platform to monitor shipping lanes and to police fisheries across the world's oceans. Moreover, in military, it could also provide a platform to track ships or to distribute a dynamic sensor array such as microphones for submarine detection [8]. So dynamic soaring has been studied extensively and some scholars have studied it intensively. Lawrance et al. [8-11] have studied autonomous soaring flight for UAV, whose contributions include the analysis of gliding flight in a structured framework and design of a path planning architecture for autonomous dynamic soaring in an unknown wind field. Besides, in order to estimate wind field for autonomous dynamic soaring, Lawrance et al. [9] provided a method for taking direct observations of the wind during flight that allowed in situ construction of a wind model. Langelaan et al. [12, 13] estimated a wind field by using a polynomial parameterization of the wind field. Bower [14] studied the energy transfer mechanisms for a vehicle flying in a spatially and temporally varying wind field. Based on the relationship between attitude and linear acceleration, Zuo [15] proposed an adaptive trajectory tracking control algorithm to estimate unknown aerodynamic parameter.

In the paper, an open-source optimal software named GPOPS (Gauss Pseudo-spectral Optimization Software) [16] is used to carry out the computation and simulation. In fact, there are a number of commercial software to investigate trajectories for dynamic soaring in specific conditions, such as AMPL, Deittert et al. [17] used to generate the optimal trajectories of UAVs in the condition of the minimal and maximal strength of wind shear for the optimal cross-country

travel. Sachs [18, 19] analysed the dynamic soaring trajectories and obtained the maximum energy transfer from the moving air to the sailplane and the minimum strength of wind shear required for albatrosses to perform dynamic soaring by ALTOS, NPSOL was used by Zhao et al. [20] to study the optimal patterns of dynamic soaring for gliders in wind shear. The valuable experiences and conclusions have inspired this paper. As many nonlinear and dynamic problems need to be solved in this study, GPOPS is more suitable. A set of differential equations are solved by using a nonlinear problem solver (SNOPT) in EQUATION. It is designed to solve multiple phase optimal control problems at a user specified number of nodes. A user can define a cost function, the dynamics equations, and connections between phases, and sets up limits and estimates for each of states and controls in GPOPS [21, 22].

Scores of research findings provide good references for this paper, especially the trajectory optimization methods of Lawrance et al. [8-11], which is very useful for studying the relationship between energy variation and optimal trajectory in dynamic soaring in this paper. In this paper, against the energy variation in the course of the dynamic soaring, the kinetics model of dynamic soaring based on gradient wind field is established. The relationship between energy variation and the change of flight parameters, mainly the relations between flight attitude angles (flight path angle and heading angle) and energy variation are analysed, and the conclusions drawn from numerical simulation are verified by flight experiment. Because dynamic soaring is normally performed at low altitudes, the purpose of this paper is to verify the aircraft can absorb enough energy from the gradient wind field by means of dynamic soaring, the conclusions of this paper about dynamic soaring at low altitudes will provide guidance for dynamic soaring at high altitudes.

The rest of the paper is organized as follows: Modelling and analysis are introduced in

Section 2. Simulation results and associated discussion are given in section 3. The results of flight experiment are presented in Section 4. Finally, the concluding remarks are made in Section 5.

2 Modelling and Analysis

2.1 The model of wind field

It is the wind shear that the aircraft uses to gain energy when following a favourable dynamic soaring trajectory. Thus, an accurate model of the wind profile is desirable.

Since the flight experiment would be carried out in Changsha (28.2°N, 112.6°E), it is necessary to build a wind field model for the experiment yard. The average strength of wind in Changsha below altitude of 100 m is shown in Figure 2, which indicates that there is a persistent wind shear, which can be explored to power the flight of aircraft by means of dynamic soaring in the range of 0~100m.

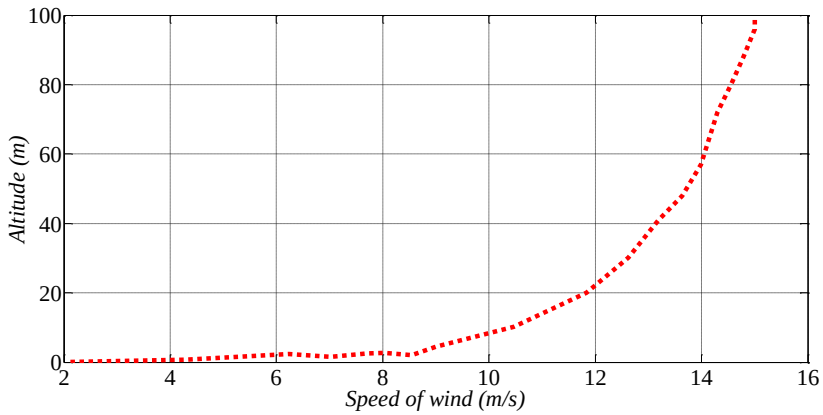

Figure 2. The observation strength of wind (0~100m) in Changsha (28.2°N,112.6°E)

From Figure 2, a logarithmic profile is chosen as this model matches the measurements near the surface of the Earth (about 0~100m). The logarithmic profile is defined as follow [23]:

$$U(z) = U_{ref} \frac{\ln(z / z_0)}{\ln(z_{ref} / z_0)} \tag{1}$$

where $U(z)$ is the wind speed at height z, and U_{ref} is the wind speed at the reference height z_{ref}. Variable z_0 is the aerodynamic roughness length or the roughness factor. It is an experimentally

derived constant that accounts for the kind of surface over which the wind is blowing. Typically, a higher value of the roughness length indicates more obstructions on the surface such as trees and buildings. In Figure 3，the fitted curve shows wind profiles for value of the roughness coefficient with U_{ref}=15m/s, z_{ref}=100m, z_0=0.05m. All these factors match well with the wind profiles near the surface of the Earth (about 0~100m) in Changsha, and are adopted throughout the remainder of this paper.

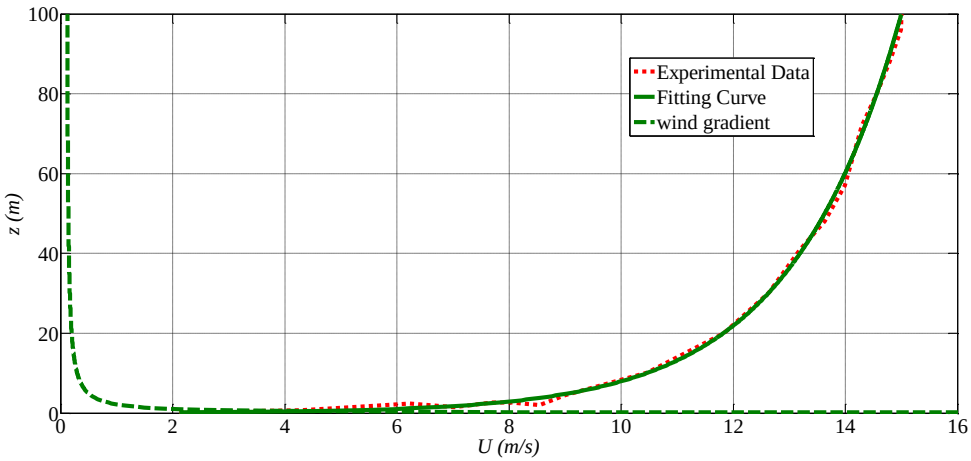

Figure 3. Wind speed vs. height

2.2 Dynamic Soaring Model

In this section the dynamic equation for a soaring aircraft in three degrees of freedom (3DOF) is discussed. In this flight model, the rotational dynamics are assumed to be significantly faster than the translational dynamics [17], and hence only translations are considered. Meanwhile, there is no propulsion system on the aircraft. For a point mass model, the forces and angles used in this model are shown in Figure 4. The inertial wind speed components in the x, y, and z directions are respectively denoted as W_x, W_y and W_z.

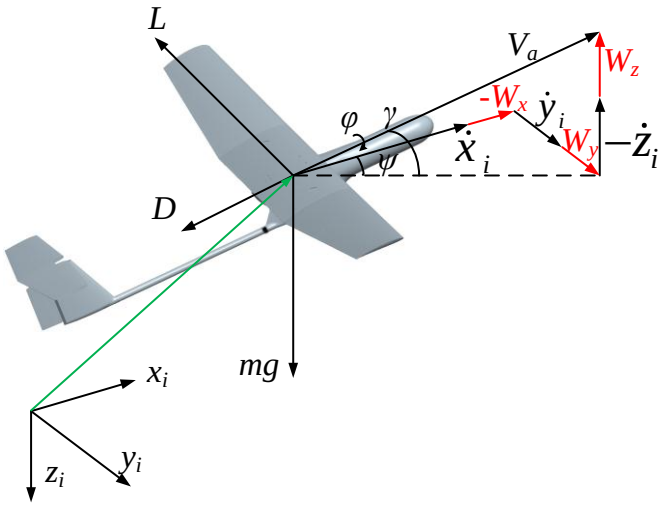

Figure 4. Air-relative velocity and applied forces for the aircraft

In Figure 4, there are three applied forces in this model accounting for: lift (L), drag (D) and gravitational force (mg); γ is flight path angle, ψ is heading angle, and φ is bank angle; V_a represents the air speed. Applying Newton's Second Law, the equations of motion are given in Equation (2).

$$\begin{bmatrix} m\ddot{x}_i \\ m\ddot{y}_i \\ m\ddot{z}_i \end{bmatrix} = \begin{bmatrix} \cos\gamma\cos\psi & \cos\psi\sin\gamma\sin\varphi - \sin\psi\cos\varphi & \cos\psi\sin\gamma\cos\varphi + \sin\psi\sin\varphi \\ \sin\psi\cos\gamma & \sin\psi\sin\gamma\sin\varphi + \cos\psi\cos\varphi & \sin\psi\sin\gamma\cos\varphi - \cos\psi\sin\varphi \\ -\sin\gamma & \cos\gamma\sin\varphi & \cos\gamma\cos\varphi \end{bmatrix} \cdot \begin{bmatrix} -D \\ 0 \\ -L \end{bmatrix} + \begin{bmatrix} 0 \\ 0 \\ mg \end{bmatrix} \quad (2)$$

i.e.

$$\begin{cases} m\ddot{x}_i = -D\cos\gamma\cos\psi + L(-\sin\gamma\cos\psi\cos\varphi - \sin\psi\sin\varphi) \\ m\ddot{y}_i = -D\cos\gamma\sin\psi + L(-\sin\gamma\sin\psi\cos\varphi + \cos\psi\sin\varphi) \\ m\ddot{z}_i = D\sin\gamma + L(-\cos\gamma\cos\varphi) + mg \end{cases} \quad (3)$$

where a dot over a variable denotes the derivative with respect to time t, and x_i, y_i, and z_i are the translational motion of the centre of gravity of the aircraft.

In the wind field, the kinematic equations of the aircraft can be expressed in Equation (4):

$$\begin{cases} \dot{x}_i = V_a\cos\gamma\cos\psi - W_x \\ \dot{y}_i = V_a\cos\gamma\sin\psi + W_y \\ \dot{z}_i = -V_a\sin\gamma + W_z \end{cases} \quad (4)$$

where $\dot{x}_i$, $\dot{y}_i$ and $\dot{z}_i$ are the absolute velocity components of the aircraft, V_a is the airspeed, W_x, W_y and W_z are the absolute velocity components of the wind.

By differentiating Equation (4) with respect to time, the following equations can be obtained:

$$\begin{cases} \ddot{x}_i = \dot{V}_a \cos\gamma\cos\psi - \dot{\gamma}V_a \sin\gamma\cos\psi - \dot{\psi}V_a \cos\gamma\sin\psi - \dot{W}_x \\ \ddot{y}_i = \dot{V}_a \sin\psi\cos\gamma + \dot{\psi}V_a \cos\psi\cos\gamma - \dot{\gamma}V_a \sin\psi\sin\gamma + \dot{W}_y \\ \ddot{z}_i = -\dot{V}_a \sin\gamma - \dot{\gamma}V_a \cos\gamma + \dot{W}_z \end{cases} \tag{5}$$

Combining Equations(3) and (5), one gets:

$$\dot{V}_a = \frac{-D - mg\sin\gamma - m\dot{W}_x \cos\gamma\cos\psi}{m} - \frac{m\dot{W}_y \cos\gamma\sin\psi - m\dot{W}_z \sin\gamma}{m} \tag{6}$$

The lift and drag forces are expressed as:

$$L = \frac{1}{2}\rho V_a{}^2 S_W C_L \tag{7}$$

$$D = \frac{1}{2}\rho V_a{}^2 S_W C_D \tag{8}$$

where ρ is air density, S_W is the wing reference area. The drag coefficient C_D is the sum of the parasitic drag coefficient C_{Dp} and the induced drag coefficient C_{Di}.[14]

$$C_D = C_{Dp} + C_{Di} \tag{9}$$

Due to the interference between the fuselage and the airfoil and the drag caused by the object and shin friction, the parasitic drag coefficient C_{Dp} can be estimated as a constant value denoted $C_{D,0}$. In this paper, after several flight experiments, the parasitic drag coefficient $C_{D,0}$ can be estimated as 0.025. The induced drag is caused by the vortices between high and low pressure regions of the lifting surface. The induced drag coefficient C_{Di} can be expressed by lift coefficient C_L as:

$$C_{Di} = \frac{C_L^2}{\pi ARe} \tag{10}$$

in which Oswald's efficiency factor e represents the deviation of the real design from the ideal elliptical wing shape, AR is the aspect ratio of the wing. The lift coefficient C_L can be solved by specifying the values as a control input.

So, the drag coefficient C_D can be expressed as:

$$C_D = C_{D,0} + \frac{C_L^2}{\pi A \mathrm{Re}} \tag{11}$$

Equations (3) can be used as a model for the simulation of an aircraft flying through a known gradient wind field. These equations can also act as constraint equations in dynamic soaring; once the ranges of altitude angles are determined, the optimized trajectory of dynamic soaring can be acquired.

2.3 Energy Equation

The primary goal of dynamic soaring is to extract enough energy from the atmosphere. This section mainly discusses the equations of energy to make the mechanism for energy transfer from the wind field to the aircraft more understandable. In the wind field, the energy variation of the aircraft is caused by the conversion between kinetic energy and potential energy, the energy gain from the wind field as well as the energy loss due to the aerodynamic drag. Other factors that affect energy variation are not discussed in the paper. So in the body-fixed coordinate system of the aircraft, the relative total energy of the aircraft is the sum of the potential energy of the aircraft and the relative kinetic energy of the air. The latter is generated by the aircraft's airspeed which is essential to keep the aircraft flying. The relative total energy is

$$E = mgz + \frac{1}{2} m V_a^2 \tag{12}$$

Differentiate the energy equation (equation12) with time, yields

$$\dot{E} = -mg\dot{z} + mV_a\dot{V}_a \tag{13}$$

It is assumed that W_y=W_z=0, and W_x increases in the form of logarithm in the altitude for the gradient wind field of the experiment ground, W_x=$U(h)$. Then

$$\frac{dW_x}{dt} = \frac{dW_x}{dz}\frac{dz}{dt} = \frac{dW_x}{dz}\left(-V_a \sin\gamma\right) \tag{14}$$

Let

$$\kappa = \frac{dW_x}{dz} \tag{15}$$

where κ is gradient of the wind. The variation trend of wind gradient profile is depicted in Figure 3.

Combining equations (13)-(15), there is:

$$\dot{E} = m\kappa V_a^2 \sin\gamma \cos\gamma \cos\psi - DV_a \tag{16}$$

It is apparent that the energy loss is mainly determined by drag (D) and the altitude angles γ and ψ play an important part in energy transformation. Equation (16) can be written as

$$\dot{E} = \dot{E}_{wind} - \dot{E}_{lose} \tag{17}$$

where $\dot{E}_{wind}$ represents the power gained from the wind field, and $\dot{E}_{lose}$ represents the power lost during the flying course. The energy extracted from the wind gradient (E_{wind}) can be represented as

$$E_{wind} = \int_0^T \dot{E}_{wind} dt \tag{18}$$

where T is the flight time of a dynamic soaring cycle.

An optimal control problem is formulated to ensure that the least energy (E_{wind}) extracted from the wind gradient can still sustain a powerless dynamic soaring flight:

$$\text{Maximum } E_{wind} \tag{19}$$

subject to Equations (3) and (5). The terminal constraints are expressed as follows

$$\gamma_{\min} \le \gamma \le \gamma_{\max} \tag{20}$$

$$\psi_{\min} \le \psi \le \psi_{\max} \tag{21}$$

$$V_{a\min} \le V_a \le V_{a\max} \tag{22}$$

$$\kappa_{\min} \le \kappa \le \kappa_{\max} \tag{23}$$

where E_{wind} is a target (cost) function, which defines the objective in dynamic soaring, to be maximised so that the energy extraction problem can be cast as a trajectory optimization problem. Equation (20) and Equation (21) together ensure that aircraft always proceeds forward along the

trajectory where the aircraft can acquire enough energy. Equation (22) defines the airspeed limits, and equation (23) is the constraint for the gradient of the wind. Equation (16) reveals the relationship between the energy loss rate and flight parameters, such as C_L, heading angle, flight path angle and so on. So, in the course of trajectory optimization, the right choice of suitable flight parameters can reduce the loss of energy.

3 Simulation and Discussion

3.1 Conversion of optimal problems

In this paper, the original optimal problem is converted into a parameter optimization using the collocation approach. This is achieved through converting the control and state histories into control and state variables [24, 25]. In equations (3) and (4), the state variables are [x_i, y_i, z_i, V_a, ψ, γ], and the control variables are [C_L, φ],

$$A=\begin{bmatrix} x_i & y_i & z_i & V_a & \psi & \gamma \end{bmatrix}^T,\ B=\begin{bmatrix} C_L & \varphi \end{bmatrix}^T \tag{24}$$

and the control variables can be expressed by

$$B=g\left(A\right) \tag{25}$$

The collocation approach needs to divide the solution time interval [t_0, t_f] of the optimisation problem by a prescribed number of time instants below:

$$t_0=t_1<t_2<\cdots t_k<\cdots<t_{N-1}<t_N=t_f \tag{26}$$

The resulting constraints at the midpoint of each node can be expressed as

$$C_k=F\left(t_m,A_m,B_m\right)=0 \tag{27}$$

where

$$t_m=\frac{t_k+t_{k+1}}{2},\ A_m=\frac{A_k+A_{k+1}}{2},\ B_m=\frac{B_{k+1}-B_k}{t_{k+1}-t_k} \tag{28}$$

By the midpoint rule of trajectory optimization, the path nodes in equation (3) are converted into a

series of discrete time points as bounds on the solution parameters.

3.2 Solutions of dynamic soaring

According to the parameters of the experimental long-endurance aircraft, the dynamic soaring model is analysed by means of MATLAB programs in this section. The toolbox used for the simulation is GPOPS [16].

The GPOPS library uses SNOPT to perform the optimization. The GPOPS case for dynamic soaring includes five scripts: a main script; a DAE (Differential algebraic equations) script; a connect script; an event script, and a cost script.

Here is a brief description of each script. The main script is the framework of the case. A dynamic soaring problem contains a number of phases, and each phase contains a section in which minimums and maximums are defined for time, states, and controls. A phase has the function to define equations of motion. The minimum and maximum values of the dynamic soaring path constraint are set in the main script. The DAE script mainly aims at the optimal control problem. All phases have one set of differential equations. The connect script contains the final states from the prior phase and the initial states for the next phase. The restriction equations are written to transform one state to another. The event script defines the partial derivatives of each event constraint with respect to the initial state, initial time, final state, final time, and parameters. Some parameters at the initial and final time are given as follows:

$$\begin{cases} V(t_0) = V_0, \quad V(t_f) = V_f \\ \psi(t_0) = \psi_0, \psi(t_f) = \psi_f \\ \gamma(t_0) = \gamma_0, \quad \gamma(t_f) = \gamma_f \\ \kappa(t_0) = \kappa_0, \kappa(t_f) = \kappa_f \end{cases} \tag{29}$$

The cost script creates the cost functions for the optimal control problem. Optimization in this paper is to seek the minimum value of the cost function.

The framework of GPOPS for path optimization is shown in Figure 5.

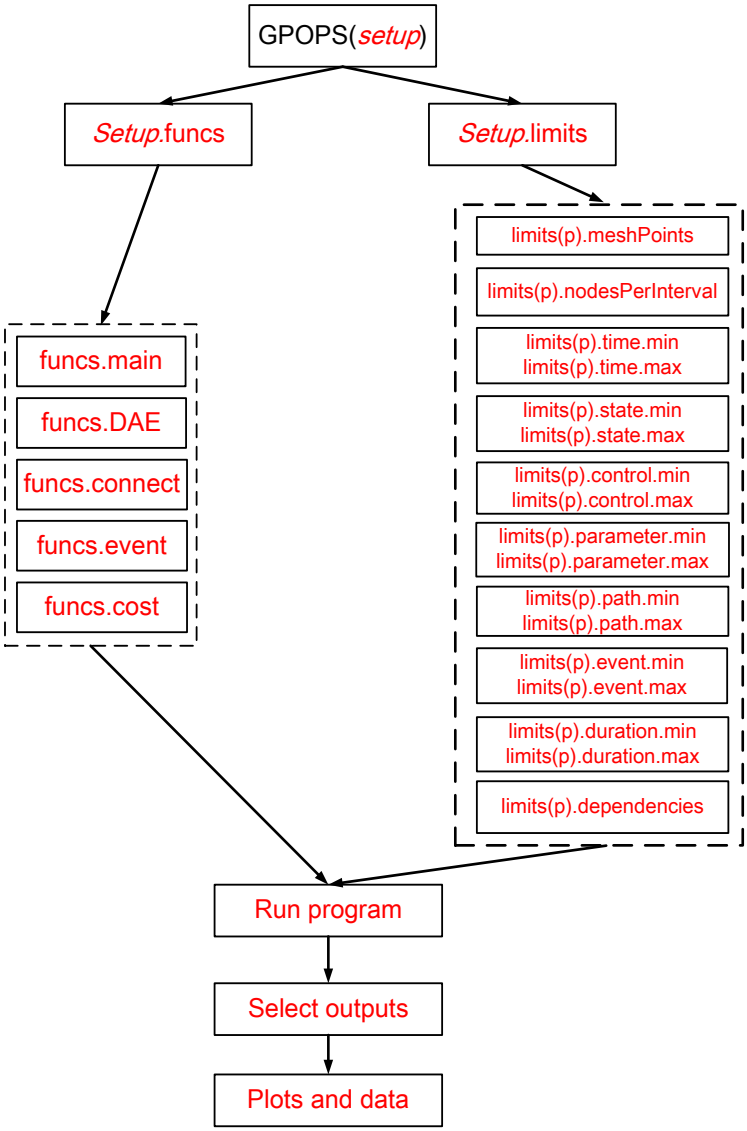

Figure 5. Mission Planning Tool Flowchart

The parameters of the long-endurance UAV demonstrator are given in Table 1.

Table 1. UAV demonstrator parameter values used

Parameter	Value
Mass [kg]	5.5
Wing Area S_w [m^2]	0.69
Aspect Ratio	16.81
Span[m]	2.61
ρ [kg/m^3]	1.22
C_{D0}	0.025

E_{max}	20

where E_{max} is the maximum lift-to-drag ratio. This is a small long-endurance aircraft, which is designed partly based on the shape of a Wandering Albatross.

First of all, under the constraints of the model, and initial and final-time conditions, the three-dimensional flight trajectory of a dynamic soaring cycle is acquired (X indicates the direction of wind), as shown in Figure 6, where black line represents the trajectory of the aircraft, red line represents the horizontal projection of the trajectory. In Figure 6, it can be seen that: in a cycle of dynamic soaring, the flying height of the aircraft is about 15m, when the gradient wind speed gap is about 5 m/s. The forward distance is about 110m. Additionally, it can be seen that in the course of turning in high altitude, the trajectory nodes are dense, the process of turning in high altitude is the most complicated energy variation phase of whole dynamic soaring. The simulation of the dynamic soaring trajectory can be used for guiding the dynamic soaring experiments.

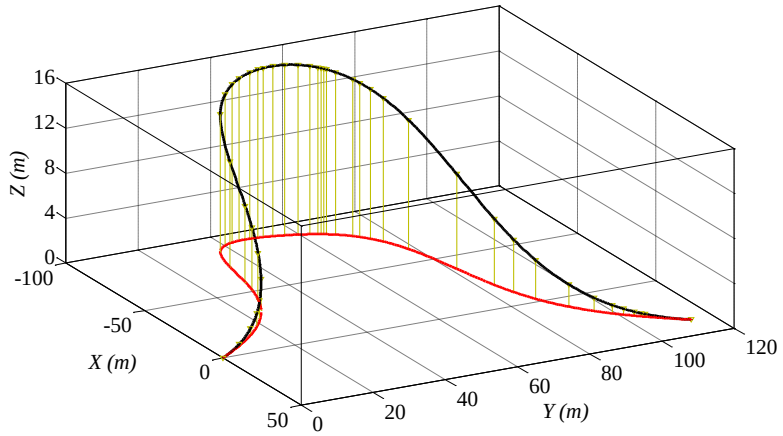

Figure 6. The simulation flight trajectory of dynamic soaring

In the simulation, the initial airspeed of the aircraft is 23 m/s. The airspeed variation in a dynamic soaring cycle is shown in Figure 7. After one cycle of flight, the airspeed is the same as the initial speed. In other words, even though there is no propulsion supplied, the aircraft can achieve flight distance by the means of dynamic soaring, despite presence of drag that consumes energy.

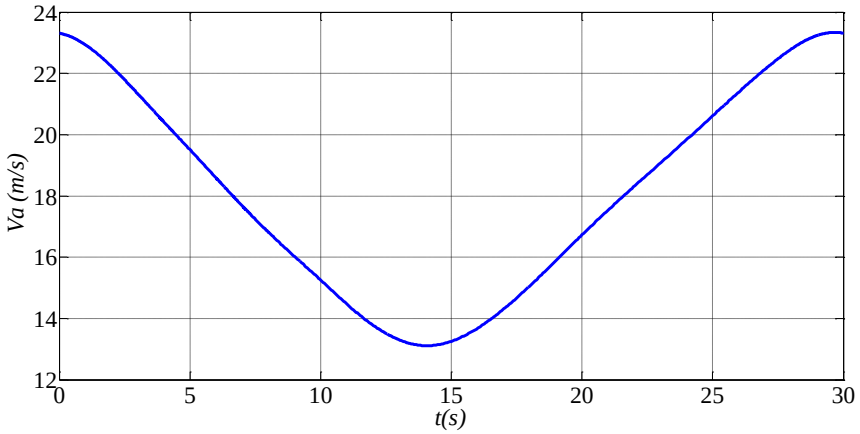

Figure 7. Airspeed for the model small UAV demonstrator flying through a log cycle

The aircraft's heading angle (ψ) and flight path angle (γ) in a dynamic soaring cycle are shown in Figure 8 and Figure 9 respectively.

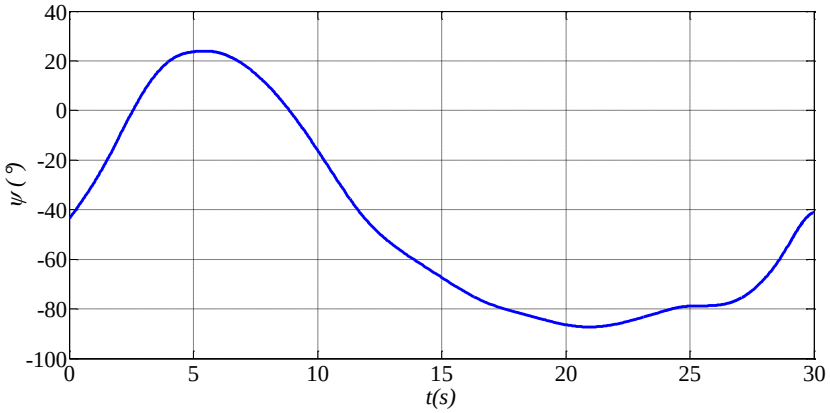

Figure 8. The heading angle (ψ) of dynamic soaring

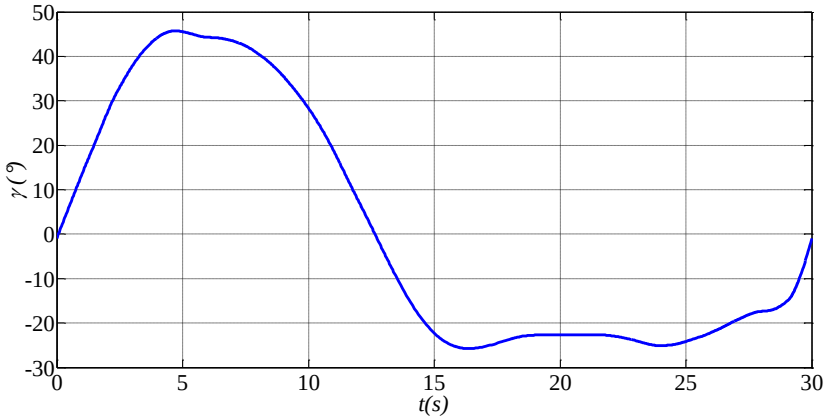

Figure 9. The flight path angle (γ) of dynamic soaring

Examining Figure 8 and Figure 9, it is clear that in the course of climbing, the aircraft's heading angle (ψ) first increases then decreases, the value ranges from [-60°，30°]. In the course

of descending, the heading angle (ψ) is steady compared with climbing. As in gliding with tailwind, the aircraft does not require too many changes of attitude angle. The variation of the flight path angle (γ) is basically the same as the heading angle (ψ), in the process of climbing, and the value of the flight path angle (γ) varies in [0°，45°]. Being consistent with the expectation of dynamic soaring model in Section 2, the aircraft continuously gains energy from the wind field during the course of climbing and turning at high altitude, but loses energy in the course of gliding with tailwind and turning in low altitude, which are expected from equation (16).

In the process of dynamic soaring, the continuous variation of attitude angles leads to the variation of lift coefficient, as shown in Figure10.

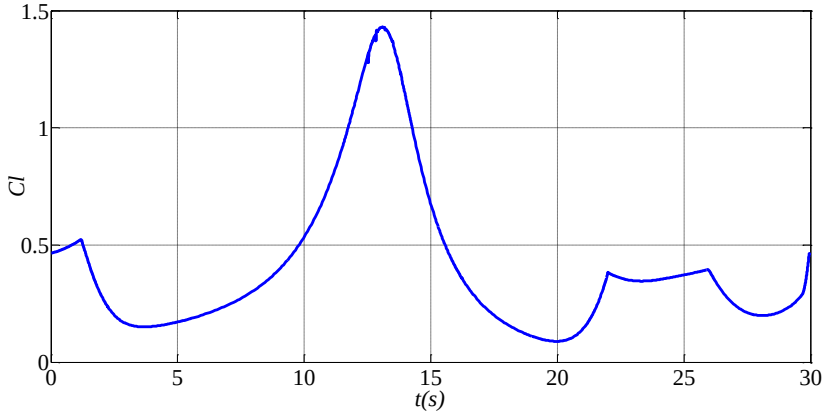

Figure 10. The lift coefficient for the model small UAV demonstrator flying through a log cycle

In Figure 10, it can be seen that the variation range of the lift coefficient is [0.2，1.5], when the aircraft get close to the peak of trajectory, both the lift coefficient and wind speed reach the maximum, and at this point, the UAV's speed becomes minimum, so that the UAV still has enough lift for flight during the turning in high altitude.

Based on the findings from the results of all parameters discussed before, and incorporated with the energy model of equation (16), the energy suction rate (dE_{wind}/dt) in the wind field can be determined, as shown in Figure 11.

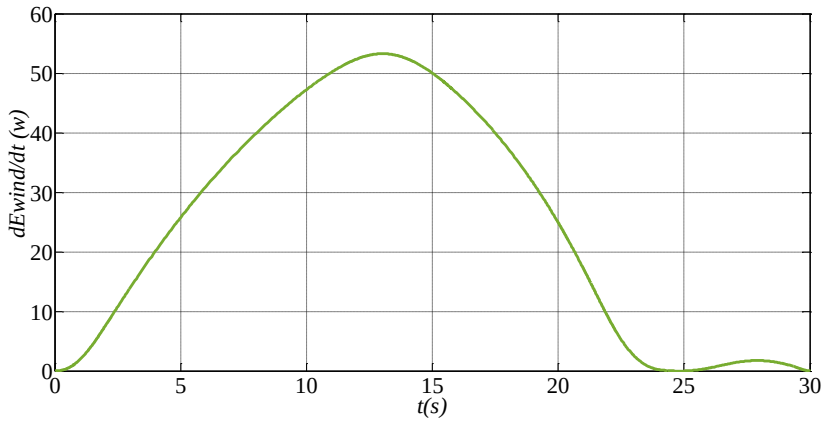

Figure 11. The power exacted from the wind for a cycle of dynamic soaring

From Figure 11, it can be found that at the beginning of dynamic soaring, the energy suction rate (dE_{wind}/dt) increases with flight height. Combined with Figure 7, the energy suction rate (dE_{wind}/dt) reaches the maximum value on the trajectory peak. After that, the energy suction rate (dE_{wind}/dt) decreases. At 25s, dE_{wind}/dt dips close to zero. So climbing with headwind and turning in high attitude are the most important processes in the whole dynamic soaring period, while gliding with tailwind and turning in low altitude are not suitable for energy extraction.

4 Experimental validation

To test the capability of the model, experiments are performed. Based on the theoretical results of the dynamic model and simulation, a dynamic soaring experiment is designed and conducted (see Figure 12). The flight experiment was carried out in Changsha (28.2^{o}N, 112.6^{o}E), and the wind field for the experiment was modeled by a logarithmic function. The wind gradient can be obtained by differentiating the logarithmic function with respect to altitude.

Figure 12. Picture of dynamic soaring experiment

The goal of the experiment is to validate the variation of airspeed, attitude angles and energy variation predicted by the theoretical dynamic model. The gradient wind field of the experiment ground is almost the same as the wind model used in the simulation, with the wind direction in the north. In the flight test, the wind gradient was not need to verify. The aircraft is equipped with the autopilot. The autopilot is fit for stabilizing and guiding a variety of UAVs, from highly functional high-speed UAVs through backpack UAVs, to hand-held micro UAVs. It supports extensive data logging and manual overrides. In the course of the experiment, the ground station of the autopilot can real-time displaying the flight parameters, the aircraft is controlled by telecommand. The initial aircraft speed is gained by the on-board engine, and then it is switched off the engine after the initial aircraft speed reached 23m/s. In the flight test, the airspeed was demonstrated by the ground station of the autopilot. The flight data is recorded by the autopilot.

After several repeated experiments, three trajectories are acquired, which are shown in Figure 13, Figure 14 and Figure 15.

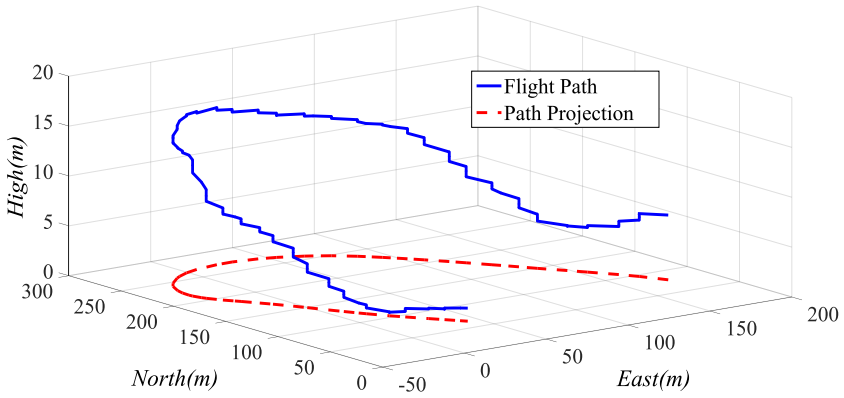

Figure13. The No.1 flying experimental trajectory

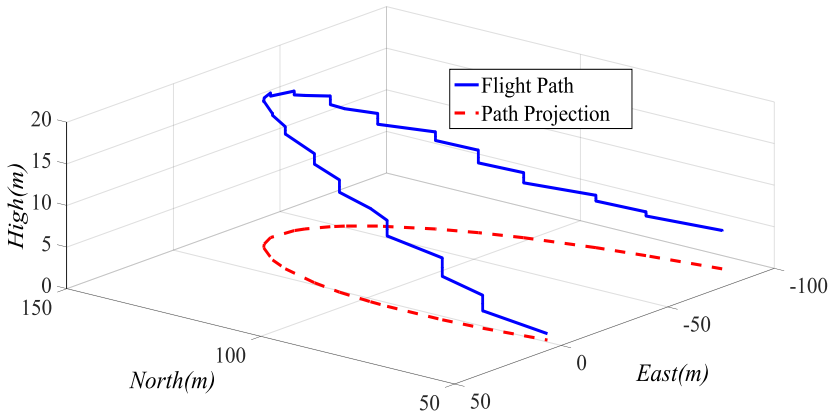

Figure 14. The No.2 flying experimental trajectory

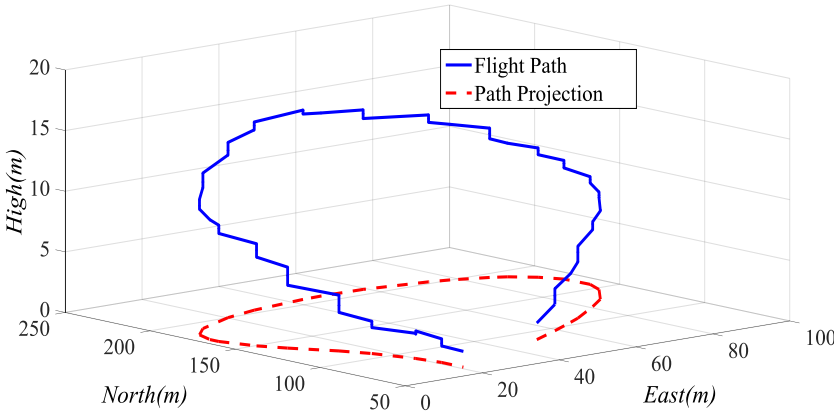

Figure 15. The No.3 flying experimental trajectory

It can be seen from Figure 13, that the flying height of the aircraft is about 15 m, and the forward distance is 110 m, which are almost the same as those of the simulation trajectory (in Figure 6). Besides comparison between the theoretical and real flying trajectories, the agreement of other parameters between the experiment and simulation should also be investigated.

By comparing Figure 16, Figure 17 and Figure 18, it can be seen that the measured airspeed and its fitted curve and the predicted airspeed in Figure 16 are quite close. During the flight experiment, the initial airspeed of the aircraft is 23 m/s, and the final airspeed is about 22.5 m/s, and the whole dynamic soaring cycle lasts about 30s.

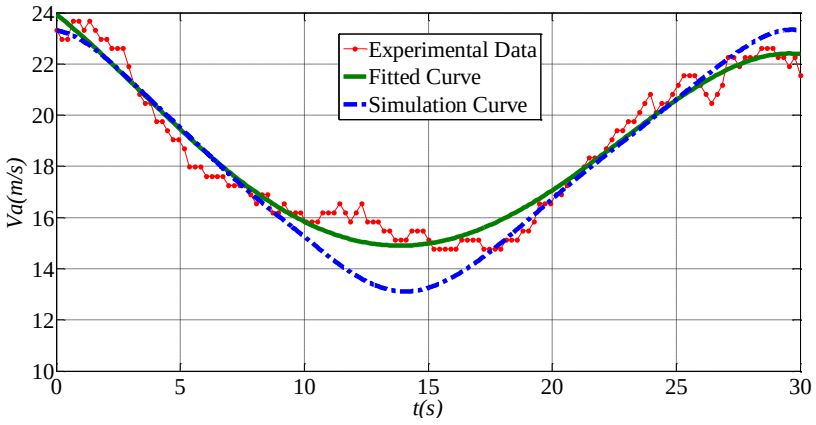

Figure 16. Airspeed for No.1 experimental UAV flying through a log cycle

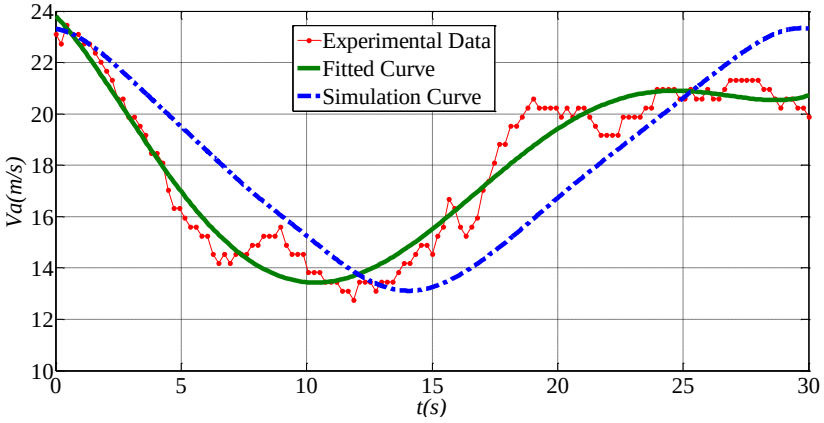

Figure 17. Airspeed for No.2 experimental UAV flying through a log cycle

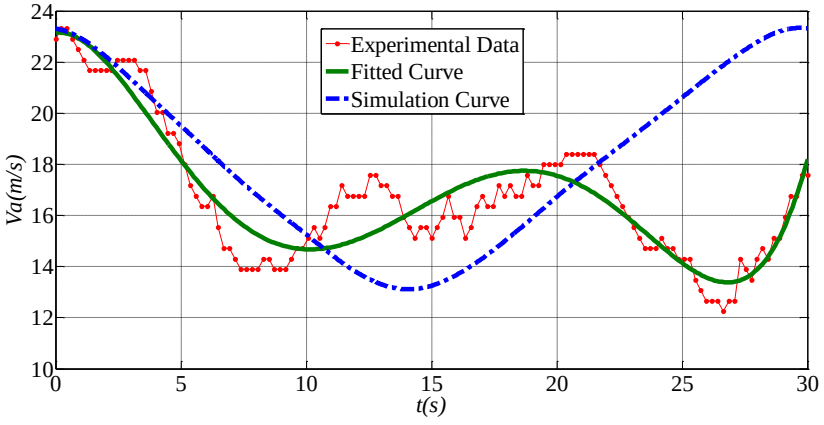

Figure 18. Airspeed for No.3 experimental UAV flying through a log cycle

Figure 16 shows that the minimum airspeed of dynamic soaring experiment is bigger than the predicted minimum airspeed. There are some differences between experimental wind field and simulation wind field, besides, the aircraft controlled by telecommand is a continuous process which is observed and adjusted by manual control. As a result, if the airspeed in the experiment is equal to or smaller than that in the simulation, the aircraft would have not enough lift to sustain flight.

In the dynamic soaring experiments, the variation of aircraft's flight path angle (γ) is shown in the Figure 19, Figure 20 and Figure 21. Compared with simulation results, the variation of flight path angle (γ) in experiment No.1 is closer to the simulation curve than the other two experiments.

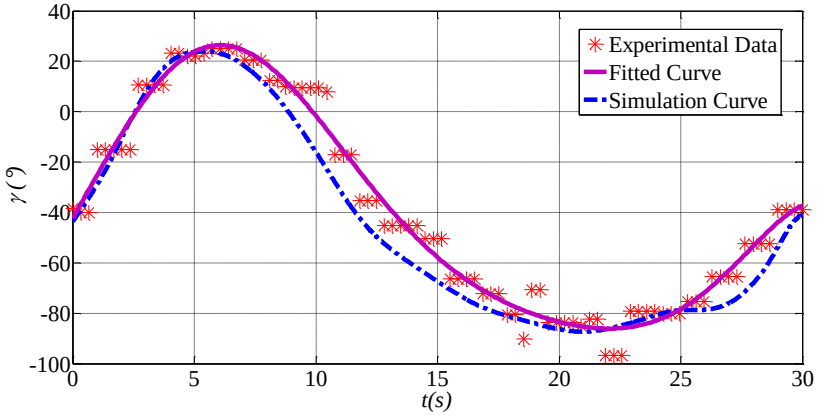

Figure 19. The flight path angle (γ) for No.1 experimental UAV flying through a log cycle

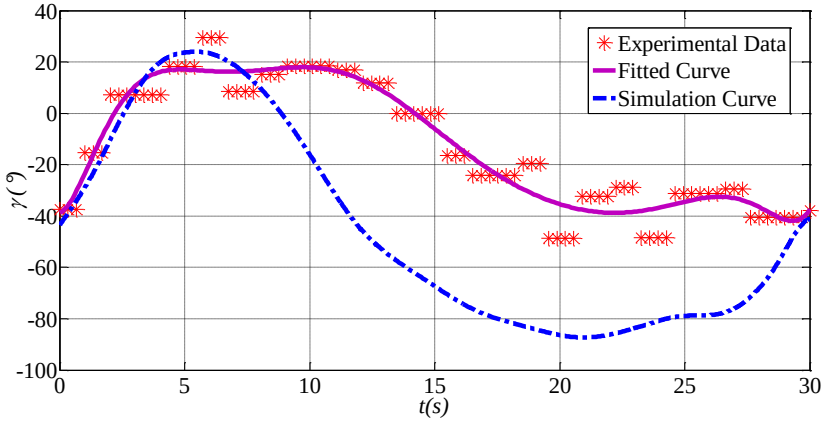

Figure 20. The flight path angle (γ) for No.2 experimental UAV flying through a log cycle

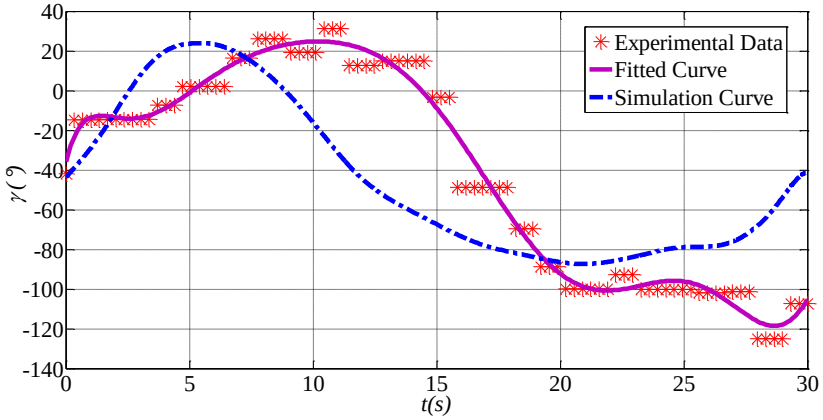

Figure 21. The flight path angle (γ) for No.3 experimental UAV flying through a log cycle

And the variation of aircraft's heading angle (ψ) is shown in the Figure 22, Figure 23 and Figure 24. Compared with the simulation curve, the variation of heading angle (ψ) in experiment No.1 is again closer to the simulation curve.

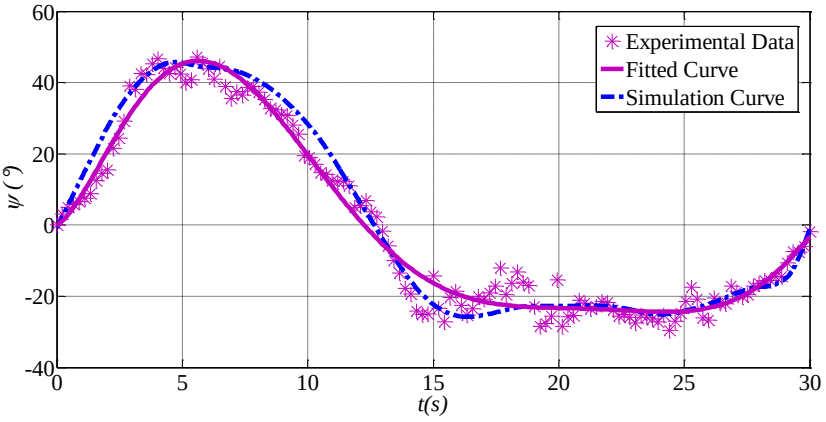

Figure 22. The heading angle (ψ) for No.1 experimental UAV flying through a log cycle

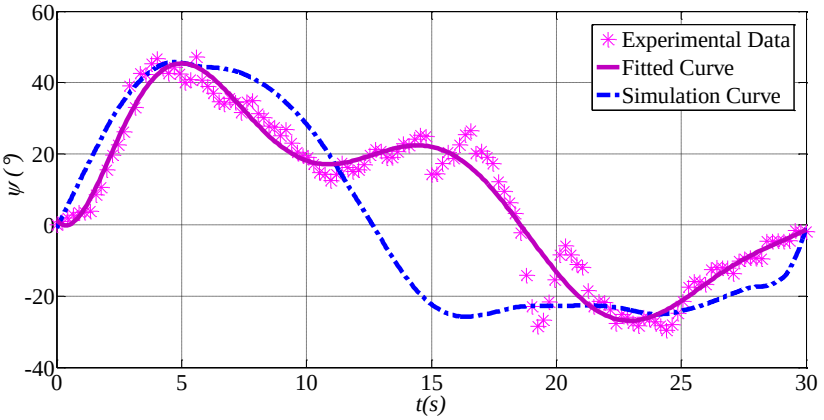

Figure 23. The heading angle (ψ) for No.2 experimental UAV flying through a log cycle

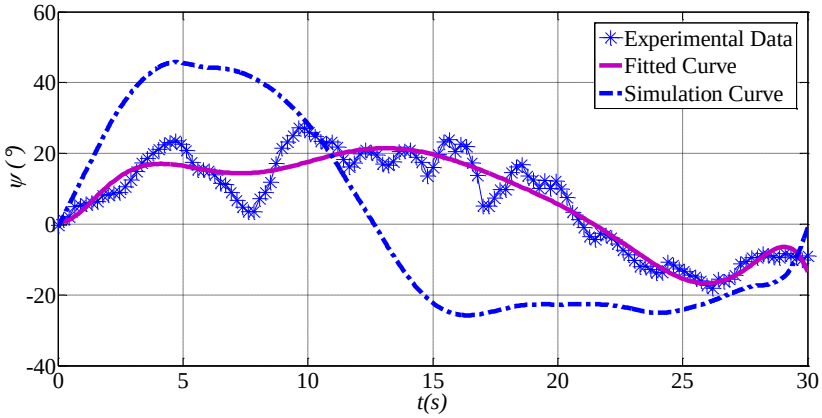

Figure 24. The heading angle (ψ) for No.3 experimental UAV flying through a log cycle

From Figure 13, Figure 16, Figure 19 and Figure 22, it can be concluded that experiment No.1 agrees well with the simulation. This seems to indicate that the dynamic model and the dynamic soaring trajectory optimization analysis are suitable for the dynamic soaring of the UAV under this study.

The detailed comparison of flying parameters between the simulation and experiments is given in Table 2 as follows:

Table 2. The comparison between simulation and experiment

	Simulation	Experiment 1	Experiment 2	Experiment 3
Initial airspeed (m/s)	23	23	23	23
Destination airspeed (m/s)	23	22.2	20.2	18
Initial height (m)	0	0	0	0
Destination height (m)	0	0.5	0.5	0.5
Difference of kinetic energy (J)	0	-99.44	-332.64	-563.75
Difference of potential energy (J)	0	27.5	27.5	27.5
Energy difference during a cycle (J)	0	-71.94	-305.14	-536.25
The farthest forward distance (m)	110	110	90	92

According to Table 2, the least energy is lost and the farthest forward distance is achieved in Experiment No.1. This is because the trajectory and flight attitude angles of Experiment No.1 matches the simulation results very well, which are optimal for energy attainment.

From the comparison between the simulation and Experiment No.1, it can be found that in the course of Experiment No.1, there is always energy lost. The major reason is that there are frictional forces between aircraft and atmosphere. Furthermore, during the soaring, the attitude of aircraft is adjusted continually by terrestrial station, which would lead to energy loss. Therefore, it is difficult to make the energy gained equal to the energy lost, although this is possible in simulation. However, in the experiments, it can be found that under the constraints of several parameters, such as flight path angle and heading angle, the aircraft can absorb energy from the wind field by means of dynamic soaring. In a word, flying without fuel is feasible. Additionally, by performing the numerical simulation, an optimized trajectory can be found which provides guidance for real flight.

5 Conclusions

This paper studies the energy transformation in dynamic soaring of the UAVs. In the process of analysis, the trajectory optimisation problem is converted into parameters optimisation using the collocation approach. The control and state histories are represented by control and state parameters. The solutions of optimal parameters are used as the guidance for flight experiments. By means of numerical simulation and experimental research, the following conclusions can be summarized:

1. The aircraft can absorb enough energy from the wind field by means of dynamic soaring. It is possible for a high-altitude UAV to fly in near space without propulsive thrust or with little power by means of dynamic soaring. If the aircraft needs to absorb enough energy to maintain flight, it should follow an optimal trajectory and take optimal attitude parameters, mainly the variation of flight path angle (γ), heading angle (ψ), which are demonstrated by simulation and experiment.

2. Theoretical analysis and flight experiments indicate that, during the early stage of dynamic soaring, the energy suction rate (dE_{wind}/dt) increases with flight height. In other words, the climbing with headwind and turning in high altitude are major phases of absorbing energy from a wind field.

In order to make UAVs capable of flying in the near space through dynamic soaring, some future work should be done, such as the accurate model of a wind field, a refined aircraft model and more dynamic soaring experiments.

Acknowledgement

This work is supported by China Scholarship Council under grant 201403170416.

References

1. Cestino E. Design of solar high altitude long endurance aircraft for multi payload & operations. *Aerospace Science and Technology*. 2006; 10: 541-550.

2. Langelaan JW and Roy N. Enabling New Missions for Robotic Aircraft. *Science*. 2009; 326: 1642-1644.

3. Bolonkin A. Utilization of wind energy at high altitude. 2004.

4. Richardson PL. How do albatrosses fly around the world without flapping their wings? *Progress in Oceanography*. 2011; 88: 46-58.

5. Wharington JM. Heuristic control of dynamic soaring. *Control Conference, 2004 5th Asian*. 2004, p. 714-722

6. Rayleigh JWS. The Soaring of Birds. *Nature*. 1883; 27: 534-535.

7. Boslough MB. Autonomous dynamic soaring platform for distributed mobile sensor arrays. *Sandia National Laboratories, Sandia National Laboratories, Tech Rep SAND2002-1896*. 2002.

8. Lawrance NRJ and Sukkarieh S. Autonomous Exploration of a Wind Field with a Gliding Aircraft. *Journal of Guidance, Control, and Dynamics*. 2011; 34: 719-733.

9. Lawrance NR and Sukkarieh S. A guidance and control strategy for dynamic soaring with a gliding UAV. *Robotics and Automation, 2009 ICRA'09 IEEE International Conference on*. IEEE, 2009, p. 3632-3637.

10. Lawrance NRJ and Sukkarieh S. Path Planning for Autonomous Soaring Flight in Dynamic Wind Fields. *2011 IEEE International Conference on Robotics and Automation*. Shanghai International Conference Center2011, p. 2499-2505.

11. NRJ L. Autonomous Soaring Flight for Unmanned Aerial Vehicles. Sydney: The University of Sydney, 2011.

12. Langelaan JW, Spletzer J, Montella C and Grenestedt J. Wind field estimation for autonomous dynamic soaring. *Robotics and Automation (ICRA), 2012 IEEE International Conference* 2012, p. 16-22.

13. Chakrabarty A and Langelaan JW. Flight Path Planning for UAV Atmospheric Energy Harvesting Using Heuristic Search. *AIAA Guidance, Navigation, and Control Conference* Toronto, Ontario Canada 2010.

14. Bower GC. Boundary Layer Dynamic Soaring for Autonomous Aircraft: Design and Validation. Stanford: Stanford University, 2011.

15. ZY Z. Adaptive trajectory tracking control design with command filtered compensation for a quadrotor. *Journal of*

Vibration and Control 2014; 19: 94-108.
16. Patterson MA and Rao AV. GPOPS − II Version 1.0: A General-Purpose MATLAB Toolbox for Solving Optimal Control Problems Using the Radau Pseudospectral Method Gainesville, FL 32611-6250 USA: University of Florida, 2013.
17. Deittert M, Richards A, Toomer CA and Pipe A. Engineless Unmanned Aerial Vehicle Propulsion by Dynamic Soaring. *Journal of Guidance, Control, and Dynamics*. 2009; 32: 1446-57.
18. Gottfried S and Orlando da C. Optimization of Dynamic Soaring at Ridges. *AIAA Atmospheric Flight Mechanics Conference and Exhibit*. American Institute of Aeronautics and Astronautics, 2003.
19. SACHS G. Minimum shear wind strength required for dynamic soaring of albatrosses. *Ibis*. 2005; 2005: 1-10.
20. Zhao YJ. Optimal patterns of glider dynamic soaring. *Optimal Control Applications and Methods*. 2004; 25: 67-89.
21. Yaple DE. Simulation and Application of GPOPS for a Trajectory Optimization and Mission Planning Tool. DTIC Document, 2010.
22. Darby CL, Hager WW and Rao AV. An hp-adaptive pseudospectral method for solving optimal control problems. *Optimal Control Applications and Methods*. 2011; 32: 476-502.
23. Ricardo B, Anouck G, Mariam A and Joo S. Shear Wind Estimation. *AIAA Guidance, Navigation, and Control Conference*. American Institute of Aeronautics and Astronautics, 2011.
24. Hull DG. Conversion of Optimal Control Problems into Parameter Optimization Problems. *Journal of Guidance, Control, and Dynamics*. 1997; 20: 57-60.
25. Seywald H. Trajectory optimization based on differential inclusion (Revised). *Journal of Guidance, Control, and Dynamics*. 1994; 17: 480-487.